2.5 THZ LASER LOCAL OSCILLATOR FOR THE EOS CHEM 1 SATELLITE

Eric R. Mueller, William E. Robotham, Jr., Richard P. Meisner, Richard A. Hart, John Kennedy, and Leon A. Newman
DeMaria ElectroOptics Systems, Inc.
1280 Blue Hills Ave.
Bloomfield, CT 06002
(806) 243-9557

Abstract

The EOS CHEM I satellite will have a channel at 2.5 THz to perform a global mapping of OH in the atmosphere. The OH data is vital to modeling of O_3 processes in the atmosphere and, in fact, OH is thought to dominate a number of cycles in the mid-latitude lower stratosphere. The OH channel will utilize two Schottky diode receivers pumped by an optically-pumped FIR laser system. DeMaria ElectroOptics Systems is presently under contract to design, fabricate, and deliver this space-based FIR laser local oscillator. The specifications, design, and modeling of this 2.5 THz laser local oscillator will be presented here, along with some of the important early design validation results.

This work is supported by Jet Propulsion Laboratory (JPL) under contract number 961080.

Introduction

In order to provide a global mapping of OH (and also $-O_2$), the Microwave Limb Sounder (MLS), on the Chem I satellite, will have channels with a LO at 2.52 THz (these channels will be collectively referred to as the THz channel). The Local Oscillator for the THz channel is a methanol laser pumped by a CO_2 laser. DeMaria ElectroOptics Systems (DEOS) leads the team that is going to deliver this laser system to JPL for integration into the MLS.

The THz channel is one of five radiometer channels on the MLS. While DEOS is providing the Laser Local Oscillator (LLO) system for the THz channel, JPL is fabricating the receivers, performing the systems integration, and conducting the atmospheric data evaluation. The spacecraft will be integrated by TRW. All of the receivers for the MLS, except the 118 & 190 GHz channels, are being fabricated by JPL.

The IF's for the THz channel are indicated in Table 1. The spectrometer for processing the IF's from all of the receivers is being developed by JPL.

Table 1: Table of IF's for the 2.52 THz Channel.

IF	Constituent
8.4 GHz	-OH
12.8 GHz	-OH
20.4 GHz	$-O_2$

While many readers may have experience with moderate-to-low reliability optically-pumped FIR lasers, high-reliability FIR lasers may not be familiar. Starting with the pump laser technology: the LLO will utilize the same high-reliability, sealed-off, RF-excited, CO_2 laser technology found in DEOS's commercial lasers and in numerous high-sophistication systems DEOS has delivered over the years. Specifically, this technology has demonstrated: operating life in excess of 35,000 hrs, shelf life of over 10 years, operation in high-performance aircraft environments, spectral purity and stability sufficient for LIDAR applications, and all within a very compact and rugged package.

Applicable vacuum and optical techniques from the CO_2 laser design are being incorporated into the FIR laser design. Thus while DEOS staff have constructed ultra-high-stability and spectral purity FIR lasers which have operated for years with only periodic gas refills, the sealing and mirror mount technologies adopted from the

CO_2 laser designs are expected to yield FIR lasers which operate for years without refilling or service of any kind.

In the design of a system as intricate, efficient, and autonomous as the LLO, a number of complex interactions, which may not be imperative for a laboratory-based system, must be considered to assure a robust design. The remainder of this paper will present the LLO design, with limited details, in the sections that follow: LLO Specifications, LLO Configuration, High-Efficiency Pump Laser, Pump Laser Frequency Control, FIR Laser, and Conclusions.

It should be pointed out that DEOS is merely the leader of the LLO team. The other team members are: Teledyne Brown Engineering – electronics fabrication, Aerospace Structural Research – mechanical/thermal design and analysis, Supplier-Based Manufacturing – quality assurance, National Technical Systems – compliance testing, and JPL – general system design guidance. The team also relies a network of vital suppliers too numerous to mention.

LLO Specifications
(abbreviated)

The LLO has a long list of specifications. In the interests of brevity only those specifications which relate to topics covered in this paper will be presented.

The LLO must autonomously operate and produce sufficient output power to optimize two Schottky diode receivers. The output power specification is 20 mW. The required lifetime is 5 years on-orbit plus 2200 hrs of ground testing. All specifications are required to be met over the entire lifetime of the LLO and thus constitute the definition of lifetime.

There are significant constraints on available prime power, mass, and envelope. The entire LLO (including all control electronics) must fit in a box no larger than 75 x 30 x 10 cm. The allowed total mass is 20 kg, and the total available 28 V DC prime power is 120 W. The size/mass/efficiency portion of the specification drives a large part of the LLO design.

Further mechanical constraints are in force via the launch survival specification. While the LLO does not have to operate during launch, it must of course survive launch. With the LLO's position on the Delta II launch vehicle, this amounts to 15.8 G RMS for 1 min on all three axes. Further, with the launch platform's acceleration profile, the time from atmospheric pressure to 1 torr is ~ 20 seconds. Therefore adequate venting must be provided to prevent rupture of non-pressure enclosures.

The frequency stability requirement is 100 kHz/s (FWHM), long-term drift not to exceed 2 MHz from line-center, and spectral purity - sidebands < -30 dBc (> 200 kHz off carrier). Since a SuperInvar structure would not be compatible with the mass budget, DEOS has devised a novel method of active frequency control for the FIR laser.

The required amplitude stability is 1% over 30 s. System level Rigrod modeling has shown this to be dominated by feedback interaction with the diplexer/receiver system. DEOS has devised a novel method to mitigate this effect as well.

The output spatial mode specification is that: only power in the specified TEM_{00} mode is counted, and the LLO output beam waist must be 4.1 mm located 465 mm from the LLO-radiator interface.

The output polarization specification is equal parts horizontal and vertical (within 10%) with any phase relationship. Thus circular polarization or 45 degree linear polarization is acceptable. 45 degree linear is the baseline for the LLO.

All of the performance specifications must be met in the presence of feedback from the diplexer/receivers. This is expected to be less than 20 %. Accordingly the specification is robustness to up to 20% FIR feedback of arbitrary phase and polarization. DEOS has devised a method to mitigate the FIR feedback, as will be presented in the FIR Laser section.

The temperature range specification for the LLO is non-trivial as well. The system will be tested from –10 to 50 C

(operational), and from –35 to 60 C (non-op survival).

LLO Configuration

The LLO block diagram is shown in Figure 1. The LLO electronically interfaces with the MLS via three main connections: prime power, RS-422 communications, and mixer bias signal.

To illustrate the operation of the LLO, "follow-the-power". Prime power is converted into RF power in the RF Power Supply. The RF power propagates through coaxial hard-line to the pump laser and excites the Pump Laser. The emitted 9.69 μm light propagates through the Pump Beam Delivery Optics and Photoacoustic Cell into the FIR Laser. Included in the

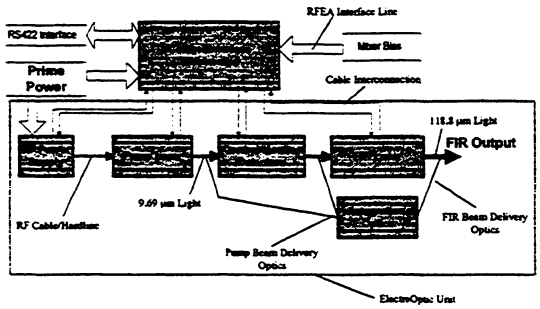

Figure 1: Block diagram of LLO.

pump beam optics are beam sample mirrors which send a very small portion of the pump power into a locking pyro and health-and-status thermopile. The FIR laser converts the pump light to FIR light at 118.83 μm (2.52 THz). Finally the FIR Beam Delivery Optics transform the laser output mode to match the specified output profile.

A drawing of the LLO is presented in Figure 2. The control/interface electronics reside in the upper portion of the housing (Control/Interface Electronics Unit), and the RF power supply and all optical components are located in the lower portion of the housing (ElectroOptic Unit). A radiator plate is mounted to the ElectroOptic unit and radiates the waste heat created by the LLO. The radiator is not structural; in fact the LLO provides the support for the radiator. The LLO's mechanical interface with the MLS is through three bipod struts (not shown) which mount to tabs shown in Figure 3.

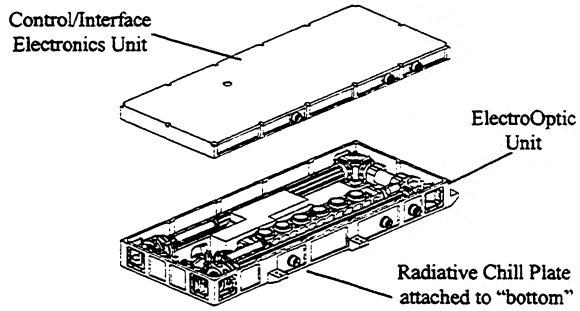

Figure 2: LLO system, enclosure opened.

The optical path for the LLO is presented in Figure 3. As shown there, the available space is quite constrained. The pump beam propagates through the Photoacoustic Cell (PA Cell) and then through the lens which focuses the beam into the FIR laser. Using crossed-Brewster-pairs to "pick-off" small portions of the

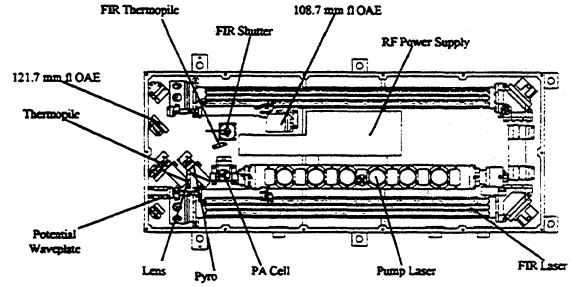

Figure 3: LLO optical path.

pump beam, beam samples are sent to the pyroelectric detector (which is used by the pump laser frequency/amplitude control electronics), and to the thermopile (pump power, health & status). Provision has been made for a ¼ λ plate, if more pump isolation is required. While this approach will yield circularly-polarized FIR output, this is compatible with the specifications.

The output from the FIR laser will be transformed to match the specified beam profile via a Newtonian telescope. This telescope is formed by two off-axis elliptical mirrors. The fastest f# in the telescope is ~7. The mirrors will be diamond-turned Al, fabricated as part of their respective optical mounts.

The FIR shutter is included to prevent a gain-switched FIR spike, possible during initial turn-on (note that if conditions

are right, the pump laser can put out a ~ 500 W pulse at turn-on), from damaging the receivers. The back of the shutter is mirrored, so that when the shutter is closed the FIR beam will propagate into the FIR thermopile (health & status). As the output telescope for the FIR beam is Newtonian, the focal spot from the telescope is an ideal location for coupling into the thermopile. This obviates the need for any additional FIR focussing element.

High-Efficiency Pump Laser

The first requirement for a high-efficiency pump laser is a high-efficiency RF power supply. In this case DEOS has already demonstrated 75 W of RF out with 100 W of DC in. The RF power supply is a conductively-cooled device that uses a class-C power amplifier stage.

While this demonstration was performed with target specifications from a Demonstration Program, DEOS now has the total LLO system design. Accordingly DEOS has reallocated power within the LLO providing 110 W of DC power to the RF power supply. With this level of input power, 85 W of RF has been demonstrated. Thus the pump laser will now have 85 W of RF pump.

Effective use of the available RF power is also key to high-efficiency operation. Through a number of patented techniques, DEOS is able to very efficiently couple the RF power into the discharge.

Diagrams of the high-efficiency pump laser are shown in Figure 4. This

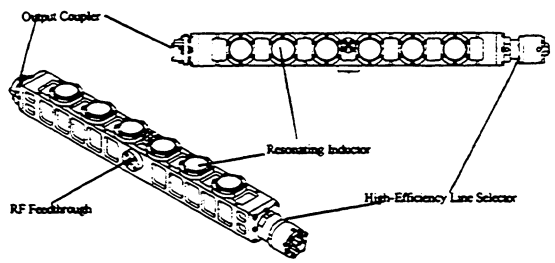

Figure 4: High-efficiency pump laser.

laser is very compact and low in mass (~ 1.5 kg). The RF circuit of the laser is formed by the combination of the electrode/waveguide/enclosure capacitance, and the resonating inductors. The RF power is admitted through a RF feedthrough in the side of the laser. The cavity is formed by the output coupler, on one end, and the high-efficiency line selector, on the other. This line selector greatly increases the efficiency of the laser, as it has an effective reflectivity at 9P36 of > 99%.

As with the entire LLO project, extensive mathematical modeling of the pump laser has been utilized. In particular, DEOS has measured Rigrod parameters for a complete distributed-loss Rigrod model[1] of the pump laser.

In the Demonstration Program, DEOS delivered an integrated pump laser/RFPS which had an output power of > 9 W @ 9P36 with 100 W of DC input. This laser also exhibited single mode operation, a property DEOS has found to be important for highest efficiency FIR operation.

It should be noted that, due to time and available optics constraints, the cavity optics in the delivered demonstration laser were not optimal. Based on the Rigrod model for the pump laser, with an optimized cavity DEOS is projecting 10 W out with 75 W of RF in. With the new internal LLO power allocations, 85 W of RF is expected – thus the projected output power from the pump laser is now 11 W.

At this time the LLO team has exposed a pump laser, of very similar design, to the launch environment and found no degradation in performance.

Pump Laser Frequency Control

Precise control of the pump frequency is essential for the LLO to meet all specifications. During the Demonstration Program the effects of operating the pump laser at its line-center were studied, as this could significantly simplify the frequency control. However it was found that operation at 9P36 line-center causes a 2 dB loss in FIR efficiency. Therefore it was decided that this would not be acceptable.

Another possible frequency control scheme would involve trying to lock the pump frequency by observing the FIR output. Careful analysis and modeling showed this to be a poor approach,

entangling numerous physical effects and making the frequency control non-robust at best.

To obtain an absolute frequency reference to lock the pump laser against, a photoacoustic cell (see Figure 5) which uses the FIR Laser vibrational pump transition in methanol,[2] was designed and tested.

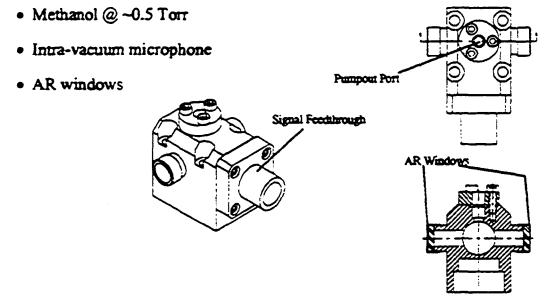

Figure 5: Photoacoustic molecular frequency standard.

The PA Cell is a very simple device. Essentially it is a sealed cavity which contains methanol at ~ 500 mtorr, a pre-polarized microphone, and AR windows. At this time the LLO team has exposed a PA Cell to the launch environment and have had

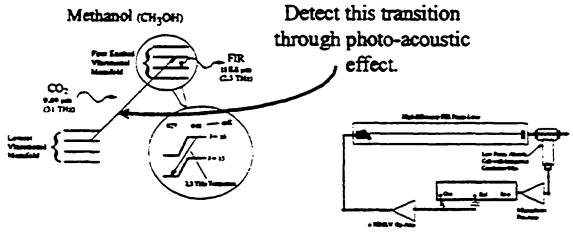

Figure 6: Pump-laser frequency locking method.

it sealed-off for over 5 months, and have observed no performance degradation.

The physical basis for the PA Cell-based pump frequency locking method is presented, graphically, in Figure 6. The pump laser is dithered about the center of the methanol absorption peak producing an acoustic signal as the amount of absorbed power is modulated. The pressure of the cell is set to be low enough that no more than 200 mW of pump power is absorbed.

While the pump laser FM will couple into the FIR output spectrum, this effect should be due to primarily two sources. The first of these, Doppler coupling induced by velocity memory effects, is given, in worst case, by

$$FM_{FIR} = FM_{pump} \cdot \frac{\nu_{FIR}}{\nu_{pump}} \qquad \text{Eq. 1}$$

where FM_{FIR}, is the Doppler-coupling-induced FIR frequency modulation, FM_{pump} is the FM dither impressed on the pump laser, ν_{FIR} is the FIR operating frequency, and ν_{pump} is the pump frequency. With the parameters for the LLO's FIR laser, the Doppler-coupling factor is ~ 1/12. Therefore the induced FIR dither will be down by a factor of 12 with respect to the pump dither. As DEOS has already demonstrated this lock with < 1 MHz of pump dither, this does not appear to be a problem with respect to the 100 kHz short-term frequency noise specification.

The above does not exhaust sources of frequency noise induced by this locking technique. There is an effect known as the two-photon-light-shift (TPLS), for standing-wave FIR lasers.[3]

This is a high-frequency, Autler-Townes,[4] Stark effect, where the Stark field is the pump field. A number of papers on this effect have been published. The LLO team has used the results in these papers to construct a model of the TPLS. While this model is not complete, it does give good agreement with the measured results for other FIR lines (there do not appear to be any direct measurements of the TPLS for the 2.52 THz line but authors[5] have indicated that the TPLS appears to be anomalously small for this transition).

The general form of the TPLS effect is given by[3]

$$\Delta\nu_{FIR} = \frac{\left[-\Delta_f - \frac{\beta^2 \cdot \Delta_p}{2\cdot\Delta_p^2 + \frac{\gamma^2}{8}}\right]}{1 + 2\cdot\pi\cdot\frac{\gamma}{c\cdot\alpha}} \qquad \text{Eq. 2}$$

where Δ_f is the FIR cavity offset from FIR line-center, γ is the vibrational & rotational (assumed same) homogenous linewidth, Δ_p is the pump laser frequency offset from the vibrational transition (in methanol) line-

center, β is the Rabi frequency for the pump transition, α is the FIR gain per unit length, and the factor in the denominator is the FIR gain-reduced pulling factor. It should be noted that β is in general proportional to the pump field magnitude (which is proportional to the square root of pump field density), and $\Delta\nu_{FIR}$ is proportional to pump power density.

As there is noticeable uncertainty in published values for the dipole matrix element,[6] and considerable inaccuracy in estimating the circulating pump intensity,[7] we estimated β from a combination of a model for circulating pump field,[8] and data obtained during the Demonstration Program.

The results of the TPLS modeling are presented in Figures 7 and 8. As shown

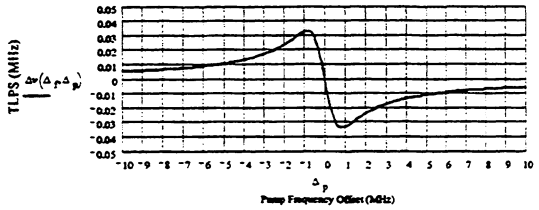

Figure 7: Two-photon light shift vs pump offset.

there the expected TPLS is 60 kHz, worst case @ 1 MHz of pump dither, and the TPLS can be minimized by operating the pump laser only slightly off of the methanol line-center. Further, as indicated earlier, an

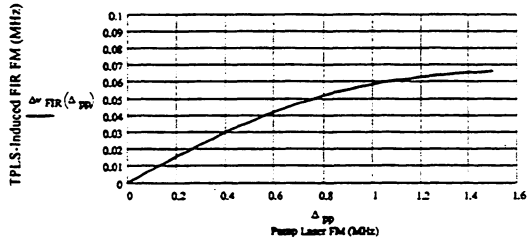

Figure 8: Worst case two-photon light shift vs pump dither amplitude.

anomalously small TPLS has been reported for the 2.52 THz laser transition.

FIR Laser

For reasons of risk[9] and schedule, the option of a ring FIR laser was dropped from the LLO early in the program. A drawing of the standing-wave FIR laser for the LLO is shown in Figure 9.

Both the input and output mirrors are mounted on PZT-actuated flexure stages. The corner mirrors are mounted on diaphragm flexure alignment mounts. The housing is aluminum with the dielectric waveguides supported inside with flexible wavesprings.

The input coupler and turn mirrors are diamond-turned copper and the input coupling is through a hole in the input mirror. The output coupler is a uniform

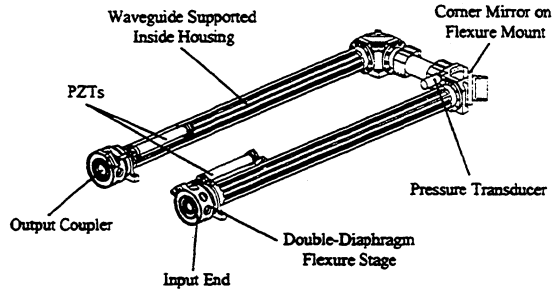

Figure 9: Standing-wave FIR laser.

capacitive mesh type coupler,[10] fabricated by the University of Massachusetts Lowell, STL & POD laboratories. Modeling of the mesh output couplers was accomplished using the GLAYERS program of CSIRO.[11]

Both the FIR modeling, and the demonstration program results showed optimal uniform output coupling to be necessary to achieve high-efficiency operation. Some of the output power vs pump power results obtained during the Demonstration Program are presented in Figure 10. All of that data was obtained

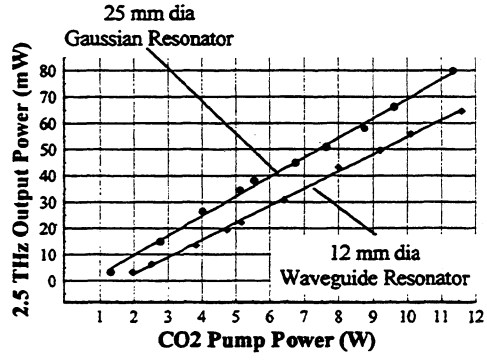

Figure 10: 1.5 m straight-guide Demonstration Program FIR results.

with the pressure held fixed at the optimal pressure for 5 W of pump power, to more accurately simulate flight conditions (ie. once sealed the FIR pressure cannot be

center, β is the Rabi frequency for the pump transition, α is the FIR gain per unit length, and the factor in the denominator is the FIR gain-reduced pulling factor. It should be noted that β is in general proportional to the pump field magnitude (which is proportional to the square root of pump field density), and $\Delta\nu_{FIR}$ is proportional to pump power density.

As there is noticeable uncertainty in published values for the dipole matrix element,[6] and considerable inaccuracy in estimating the circulating pump intensity,[7] we estimated β from a combination of a model for circulating pump field,[8] and data obtained during the Demonstration Program.

The results of the TPLS modeling are presented in Figures 7 and 8. As shown

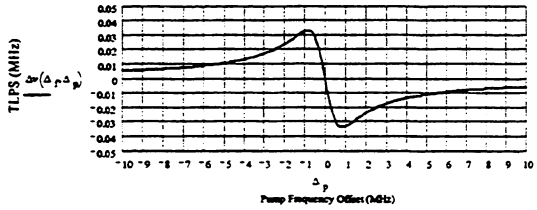

Figure 7: Two-photon light shift vs pump offset.

there the expected TPLS is 60 kHz, worst case @ 1 MHz of pump dither, and the TPLS can be minimized by operating the pump laser only slightly off of the methanol line-center. Further, as indicated earlier, an

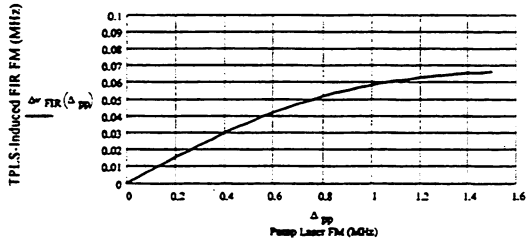

Figure 8: Worst case two-photon light shift vs pump dither amplitude.

anomalously small TPLS has been reported for the 2.52 THz laser transition.

FIR Laser

For reasons of risk[9] and schedule, the option of a ring FIR laser was dropped from the LLO early in the program. A drawing of the standing-wave FIR laser for the LLO is shown in Figure 9.

Both the input and output mirrors are mounted on PZT-actuated flexure stages. The corner mirrors are mounted on diaphragm flexure alignment mounts. The housing is aluminum with the dielectric waveguides supported inside with flexible wavesprings.

The input coupler and turn mirrors are diamond-turned copper and the input coupling is through a hole in the input mirror. The output coupler is a uniform

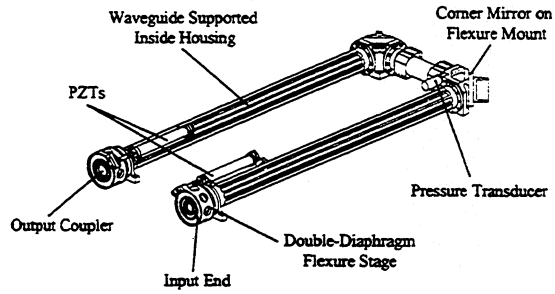

Figure 9: Standing-wave FIR laser.

capacitive mesh type coupler,[10] fabricated by the University of Massachusetts Lowell, STL & POD laboratories. Modeling of the mesh output couplers was accomplished using the GLAYERS program of CSIRO.[11]

Both the FIR modeling, and the demonstration program results showed optimal uniform output coupling to be necessary to achieve high-efficiency operation. Some of the output power vs pump power results obtained during the Demonstration Program are presented in Figure 10. All of that data was obtained

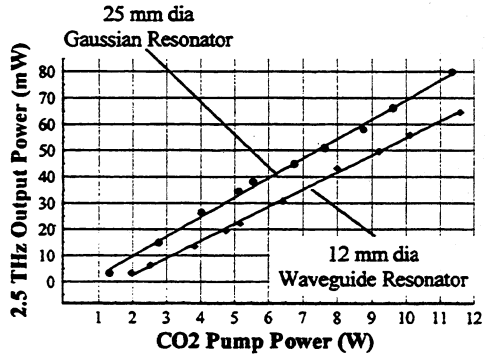

Figure 10: 1.5 m straight-guide Demonstration Program FIR results.

with the pressure held fixed at the optimal pressure for 5 W of pump power, to more accurately simulate flight conditions (ie. once sealed the FIR pressure cannot be

adjusted therefore optimization at the low end of pump power is prudent). The results in Figure 10 bracket the cavity geometries required to meet the initial internal goal of 20 mW out with 5 W of pump power. In looking at Figure 10, it should be remembered that the delivered pump laser actually had an output power of > 9 W – thus a great deal of margin was demonstrated.

The results of Figure 10 are for a straight-guide laser and the losses associated with cavity turns are expected to reduce efficiency and improve mode selection. DEOS developed a distributed-loss Rigrod model for the FIR laser. The results of this model with 5 W of pump are summarized in Figures 11 –13.

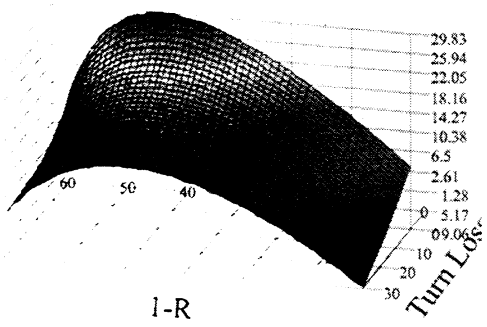

Figure 11: Rigrod prediction for FIR output vs turn loss and output coupling. Pump power fixed @ 5 W.

Figures 11 and 12 plot the output power vs output coupling and turn loss, with

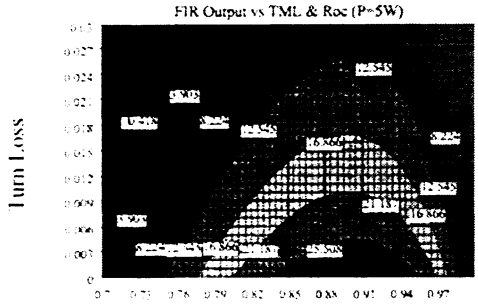

Figure 12: Rigrod prediction for FIR output vs turn loss and output coupling. ("Plan View") Pump power fixed @ 5 W.

the pump power fixed at 5 W. Figure 13 presents the output power vs turn loss with the output coupling fixed at 9 %, and the pump power fixed at 5 W.

All of the parameters for the Rigrod model were determined experimentally during the Demonstration Program. There were no adjustable parameters at this stage of the modeling effort. The most important conclusion of these figures is that turn loss is the key to high-efficiency operation. The LLO's FIR laser operates in the low-gain low-loss regime, thus any loss is significant. Although not shown in this paper, the experimental results for a folded FIR laser show the threshold regime to be below 5 W of pump power – thus the LLO's FIR laser will not be operating in the threshold regime.

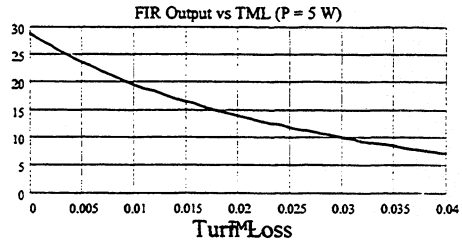

Figure 13: Rigrod prediction for FIR output vs turn loss. Output coupling fixed at 9%, pump power fixed @ 5 W.

The issue of FIR feedback from the diplexer/receivers, combined with the schedule & performance risks of associated with a ring laser, has directed the LLO program towards a novel method for feedback mitigation. Figure 14 illustrates the basis for the approach.

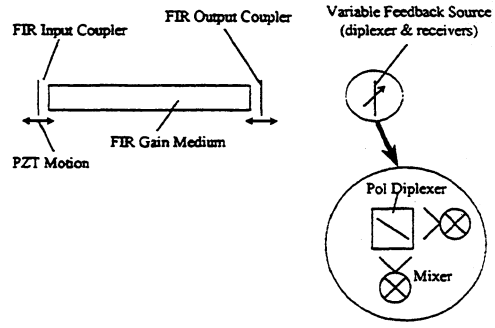

Figure 14: FIR feedback mitigation approach.

The feedback can be considered as a part of the FIR output coupler. This is effectively an etalon output coupler whose reflectivity and effective phase shift are given by

$$E_r(L_{cc}, R_{oc}, R_{fb}) := \sqrt{R_{oc}} - \frac{\left[e^{-i\cdot 4\pi\cdot\frac{L_{cc}}{\lambda}}\cdot\left(\sqrt{1-R_{oc}}\right)^2\cdot\sqrt{R_{fb}}\right]}{1-\sqrt{R_{oc}}\cdot\sqrt{R_{fb}}\cdot e^{-i\cdot\left(4\pi\cdot\frac{L_{cc}}{\lambda}\right)}}$$

Eq. 3

$$\phi := \arg(E_r)$$

Eq. 4

where E_r is the reflected complex E field seen at the output coupler, L_{cc} is the "coupled-cavity" length, R_{oc} is the reflectivity of the output coupler, R_{fb} is the feedback reflectivity, λ is the FIR wavelength, and ϕ is the effective phase seen at the output coupler.

A signal from one of the mixer bias lines will be fed into the LLO control electronics and used to optimize the output power at all times. Since the LLO control electronics have the ability to command both cavity end mirrors, and the pump laser is locked to an absolute reference, the FIR frequency can be assured to be at line-center.

Effects of this control strategy have been modeled and are presented in Figure 15. Figure 15 (a) shows the frequency pulling as a function of change in "coupled-cavity" length (Δl, distance between the diplexer/receivers and the FIR output coupler) and feedback percentage. Figure 15 (b) shows the effective reflectivity vs Δl and feedback percentage. Figure 15 (c) shows the FIR output power vs Δl and turn loss at a fixed pump power of 5 W.

These figures demonstrate:

- FIR feedback results in both frequency and amplitude pulling
- Reflectivity pulling drives the efficiency
- The magnitude of the effects increase rapidly with increasing feedback percentage

Further analysis also reveals that the FIR feedback acts most strongly in amplitude and second in frequency.

The LLO control design is using the results of the feedback modeling in both design and modeling of the control system (loop margins, etc.).

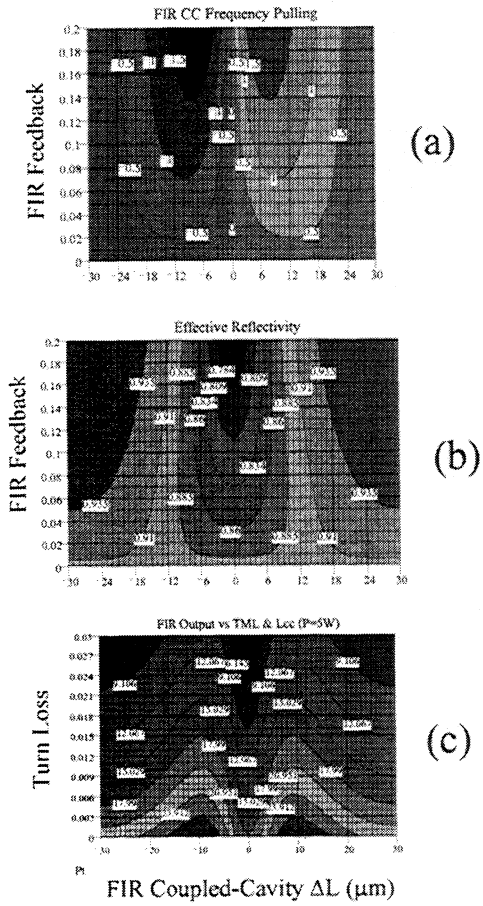

Figure 15: FIR feedback control effects. (a) FIR frequency pulling [MHz] vs FIR feedback and change in "coupled-cavity" length (Δl), (b) effective output coupling vs FIR feedback Δl, (c) predicted FIR output vs turn loss and Δl, pump fixed @ 5 W.

To test the FIR models, and then later to improve them, a high versatility testbed laser was constructed. Figure 16 shows the external and internal view of the testbed laser. Figure 17 shows some more detailed views of the internal workings of the laser.

The testbed is an aluminum enclosure housing a SuperInvar plate on which all of the optical stages are mounted. Cavity translation is accomplished via a 180 μm PZT mounted in a vacuum-tight "can" (see Figure 17 (c)). The inside of this can is kept at atmospheric pressure to avoid discharge problems.

A wide range of waveguide diameters can be used in this laser and easily changed, as they are not involved in the vacuum seal.

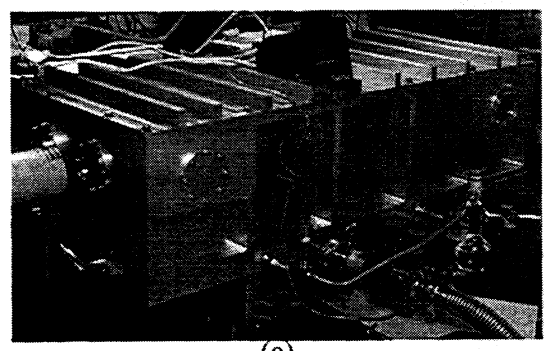

(a)

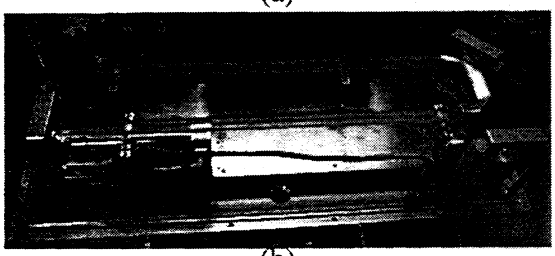

(b)

Figure 16: FIR testbed laser. (a) external view, (b) internal view.

The testbed laser also has two ports at each corner to enable virtually any cavity configuration. In a different hardware program, where DEOS is developing a compact high-power FIR laser for another application, the testbed laser will be used to test different ring laser options.

The miter, which holds the three guide pieces together, is shown in Figure 17 (b). As seen there and in Figure 17 (a), the waveguide sections are held in precision-machined V-blocks by standard coil springs stretched across the guide sections. All four of the gimbal stages are slightly modified commercial units.

The testbed laser has sufficient vacuum integrity to permit sealed off operation for many hours and in fact the pressure is typically observed to decrease with time as a result of methanol adsorption onto the internal surfaces. The pressure is monitored by a standard Pirani gauge. While this gauge's calibration is a function of gas composition, it is not prone to drift, and is quite hardenable for flight applications. The LLO will use a custom Pirani gauge to monitor the FIR laser pressure.

The results obtained with the testbed laser are presented in Figure 18 along with a comparison to the model results that were included in our LLO proposal. As observed in Figure 18, the experimental results are within 9 % of the original prediction. This

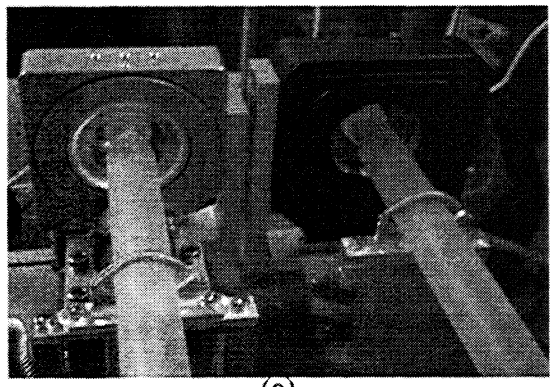

(a)

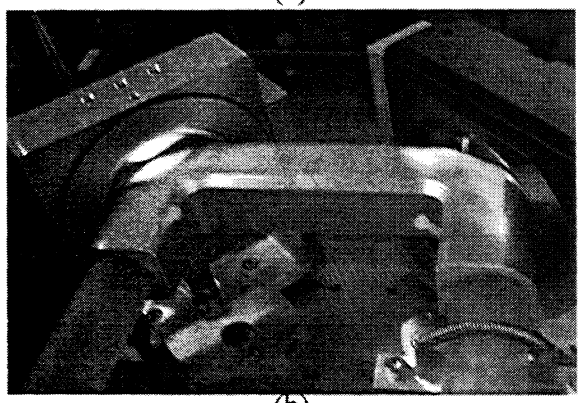

(b)

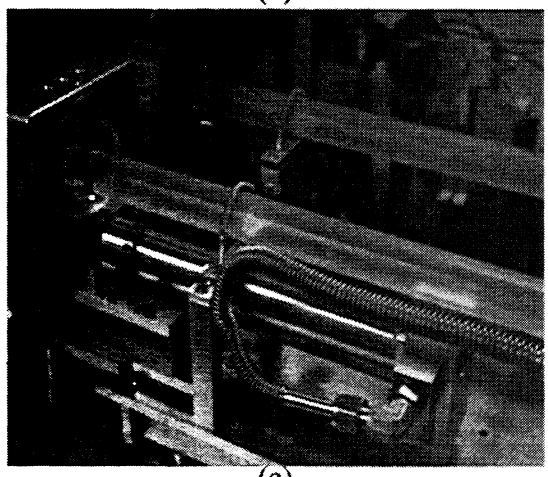

(c)

Figure 17: FIR testbed laser internal details. (a) input/output end, (b) turn end, (c) PZT "can" cavity length adjustment.

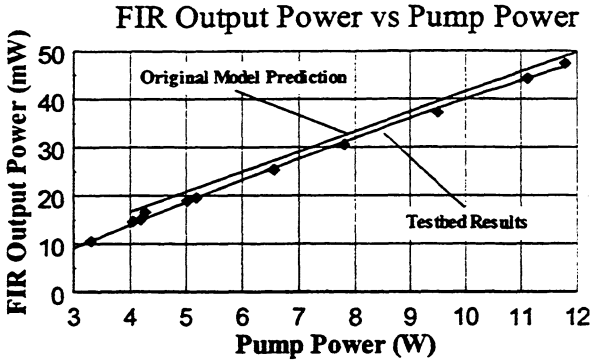

Figure 18: Testbed results: comparison with original model.

prediction was based on an estimate for the turn loss of 0.8 %/turn (reflectivity loss + guide-guide loss around the turn as a result of the unguided region of the mitered corner). If one now takes the Rigrod model and treats the turn loss as an adjustable parameter, then with a turn loss of 1.2 %/turn the model falls directly over the experimental data.

To provide lifetime confidence, DEOS is constructing a simple straight-guide FIR laser system, which uses identical stages, materials, and sealing techniques to those employed in the LLO. This laser system will be operated continuously up to, and possibly after, launch of the Chem I satellite. Thus at the time of launch, there will be > 2 years of lifetime data accumulated.

As a backup option, if any long-term FIR gas degradation issues arise, the LLO design is carrying an optional pump-fill molecular-sieve system. This system uses space proven molecular-sieve technology where one sieve is to be used as a exhaust-free pump, and the other as a source sieve. Calculations indicate that such a system should provide >1000 laser refill cycles (once every 2 days over the total required life). With the assistance of Rutherford Appleton Laboratory, the LLO team is presently designing the molecular sieves.

Conclusions

The LLO will utilize high-reliability laser technology to meet the needs of the MLS for Chem I. There will be substantial performance margin at delivery and thorough modeling for the entire LLO including control electronics. At the time of launch, >2 years of lifetime data for the LLO will have been accumulated.

FIR feedback effects will be mitigated through the use of a "coupled-cavity" control architecture.

Based on already demonstrated results, the LLO team is projecting 43 mW of FIR output at system delivery.

Acknowledgements

The authors wish to acknowledge the vital contributions of the network of suppliers, and of the other team members, to this work. This work is supported by NASA's Jet Propulsion Laboratory under contract number 961080.

[1] W. W. Rigrod, IEEE JQE, Vol. QE-14(5), 377 (1978)
[2] G. Busse, E. Basel, and A. Pfaller, Appl. Phys., Vol. 17, 387 (1977)
[3] C. R. Pidgeon, W. J. Firth, P. A. Wood, A. Vass, and B. W. Davis, Int. J. IR & MMW, Vol. 2(2), 207 (1981); S. T. Shanahan, and N. R. Heckenberg, Opt. Commun. Vol. 50(6), 393 (1984)
[4] S. H. Autler, and C. H. Townes, Phys. Rev., Vol. 100, 703 (1955)
[5] P. M. Plainchamp, IEEE JQE, Vol. QE-15(9), 860 (1979)
[6] J. Heppner, C. O. Weiss, U. Hubner, and G. Schinn, IEEE JQE, Vol. QE-16(4), 392 (1980); S. T. Shanahan, and N. R. Heckenberg, Opt. Commun. Vol. 50(6), 393 (1984)
[7] A. Harth, Int. J. of IR & MMW, Vol. 12(3), 221 (1991)
[8] J.-M. Lourtioz, and R. Adde, J. Physique, Vol.41, 251 (1980)
[9] J. H. Lee, C. L. Rettig, N. C. Luhmann, JR., and W. A. Peebles, Rec. Sci. Instrum. Vol. 63(10), 4678 (1992)
[10] R. Densing, A. Erstling, M. Gogolewski, H-P Gemund, G. Lundershausen, and A. Gatesman, Infrared Phys., Vol. 33(3), 219 (1992)
[11] P. A. Stimson, and L. B. Whitbourn, "GLAYERS, A Program for the IBM PC which Calculates the Properties of Metal Grids in Dielectric Stacks," (1989)